SPi	Journal Code:				Article ID	Dispatch: 00.00.00	CE: MAS
	J	G	R	F	21130	No. of Pages: 20	ME:

Revised proofs are sent only in the case of extensive corrections upon request.

AGU100 ADVANCING EARTH AND SPACE SCIENCE

JGR Earth Surface

RESEARCH ARTICLE

10.1029/2019JF005286

Key Points:

- Bank roughness in the shape of periodic bumps provides the controlling factor for river widening
- We develop a physics-based model that is able to predict the equilibrium cross section for rivers at the bankfull condition
- The model provides an unifying interpretation for both gravel and sand bed rivers

Correspondence to:
S. Francalanci,

Citation:
Francalanci, S., Lanzoni, S., Solari, L., & Papanicolaou, A. N. (2019). Equilibrium cross section of river channels with cohesive erodible banks. *Journal of Geophysical Research: Earth Surface*, *124*. https://doi.org/10.1029/2019JF005286

Received 2 AUG 2019
Accepted 9 DEC 2019

Equilibrium Cross Section of River Channels With Cohesive Erodible Banks

S. Francalanci [1], S. Lanzoni[2], L. Solari[1], and A. N. Papanicolaou[3]

[1]Department of Civil and Environmental Engineering, University of Florence, Florence, Italy, [2]Department ICEA, University of Padova, Padova, Italy, [3]Department of Civil and Environmental Engineering, University of Tennessee, Knoxville, TN, USA

Abstract Predicting the equilibrium cross section of natural rivers has been widely investigated in fluvial morphology. Several approaches have been developed to meet this aim, starting from regime equations to the empirical formulations of Parker et al. (2007) and Wilkerson and Parker (2011), who proposed quasi-universal relations for describing bankfull conditions in sand and gravel bed rivers. Nevertheless, a general physics-based framework is still missing, and it remains an open issue to better clarify the basic mechanisms whereby a river selects its width. In this contribution we focus our attention on lowland rivers with cohesive banks, whose resistance to erosion is crucial to control the river width. In particular, we formulate a theoretical model that evaluates the equilibrium width of river cross sections modeling the interaction between the core flow in the central part of the section and the boundary layer that forms in the correspondence of the cohesive banks. The model computes the cross-section equilibrium configuration by which the shear stresses on the banks equal a critical threshold value. These stresses are computed by partitioning the total shear stress into an effective grain roughness component and a form component (Kean and Smith, 2006a). The model is applied to a large data set, concerning both sand and gravel bed rivers, and it is used to determine the relations expressing the channel width and the bankfull flow depth to the bankfull discharge, which appear to provide a unitary description of bankfull hydraulic geometry.

1. Introduction

Predicting the equilibrium cross section of natural rivers has attracted the attention of many researchers for a long time. Field and laboratory observations were initially used to derive empirical methods, known as *regime equations*, to be used as simple predictive tools (Blench, 1957; Inglis, 1949; Lacey, 1930; Lane, 1955; Lindley, 1919; Simons and Albertson, 1963). In particular, Leopold and Maddock (1953) expressed the channel width, the average flow depth, and the average flow velocity as functions of the annually averaged flow discharge. The regime equations were also derived by means of the extremal hypothesis approach, which is based on maximizing (or minimizing) some channel function. Examples in this sense include maximizing sediment transport capacity (Pickup, 1976; White et al., 1982) or friction factor (Davies and Sutherland, 1980), or minimizing stream power (Chang, 1979, 1980a, 1980b), production of entropy (Leopold and Langbein, 1962), rate of energy dissipation (Yang et al., 1981), or Froude number (Yalin and Ferreira Da Silva, 2000). Even though these regime methods provide predictions of channel geometry in reasonable agreement with a large range of field observations, the extremal hypothesis assumption is not founded on a fully convincing physical explanation and, hence, has been subject to many criticisms (Darby and Thorne, 1995; Griffiths, 1984; Ferguson, 1986; Knighton, 1998; Mosselman, 1998).

The weaknesses of empirical methods encouraged the formulation of new physics-based approaches. A rational method was first developed following the assumption that a stable channel forms when a threshold condition for sediment motion establishes along the whole cross-section boundary (Glover and Florey, 1951; Lane, 1955). This methodology was later revised and improved by Colombini and Tubino (1991) and Diplas and Vigilar (1992), who reformulated the problem by considering the unknown bank shape as part of the solution, and Cao and Knight (1998), who included the effect of secondary flow. In the case of gravel bed rivers, a mechanistic approach was used to explore the physical mechanisms responsible for shaping the equilibrium cross section in the presence of a nonvanishing sediment transport. The so called *stable-channel*

paradox, whereby the bank regions are stable while sediment are transported as bed load in the central portion of the river cross section, was resolved by Parker (1978a) by accounting for the lateral transfer of longitudinal momentum due to turbulence. The resulting distribution of cross-sectional bed shear stresses is such that stresses are highest in the central cross-section region, where bed load transport occurs, whereas at the bank toe the shear stress reaches the critical value for the onset of sediment motion Parker (1978a). In the case of sand-bed rivers, the problem of an equilibrium section allowing the transport of sediment as both bedload and suspended load in its central part was tackled by Parker (1978b), who imposed a balance between the two lateral sediment load fluxes. Extensions of this strategy to solve the stable channel paradox were subsequently proposed by Ikeda et al. (1988), who considered the case of gravel bed rivers with heterogeneous sediment, and Ikeda and Izumi (1991), who focused on straight sand rivers.

The widening of straight channels until a stable cross section is attained has been simulated numerically by Pizzuto (1990), who applied the modified area procedure of Lundgren and Jonsson (1964) to derive the cross-sectional distribution of bed shear stresses. The channel bed topography was then derived according to the sediment flux balance equation and a heuristic bank failure law, based on exceeding the sediment repose angle. The adoption of a fully nonlinear vectorial formulation of bed load transport, allowed Kovacs and Parker (1994) to simulate continuously the widening of the channel up to equilibrium without introducing any empirical bank collapse law.

More recently, taking advantage of a comprehensive data set concerning single-thread gravel-bed rivers, Parker et al. (2007) used regression analysis to derive a set of "quasi-universal" dimensionless relations, expressing bankfull hydraulic geometry (width and average flow depth) as a function of the bankfull flow discharge. A similar set of relations was later developed by Wilkerson and Parker (2011) for sandy rivers. Blom et al. (2017), while investigating the equilibrium configurations of rivers under variable flow, proposed two relationships relating channel slope, width and bed sediment composition to given liquid and solid input distributions. The influence of sediment supply on the equilibrium channel geometry of gravel rivers was also investigated by Pfeiffer et al. (2017).

Despite the large number of approaches proposed in the literature, a unified and common framework able to explain the equilibrium width for both sand-bed and gravel-bed rivers is still missing. In this work, we try to fill this gap by developing a physics-based model that predicts the equilibrium bankfull width of natural rivers with cohesive erodible banks. Here, we use the term *cohesive* to denote banks characterized by a sediment (or a mixture of sediments) with a critical shear stress for fluvial erosion that is different and generally higher than that of the sediment composing the channel bed. Figure 1 shows a typical example of the river cross section we are dealing with: In the specific case it is a gravel-bed river, the Cecina (Italy), with composite river banks. In particular, Figure 1a highlights the presence on the bank surface of a sequence of wavy macroroughness elements (bumps), which have been found to be typical of a number of rivers (Darby et al., 2010; Kean and Smith, 2006a; Nardi and Rinaldi, 2010). They play a fundamental role in the present modeling approach, since they control the skin friction responsible for bank erosion (Kean and Smith, 2006a). The resistance to bank erosion can thus be parameterized on the basis of the bump geometry (mean height and wavelength) and the critical shear stress for sediment erosion, which usually depends on grain size, on the cohesion properties of the material composing the banks, and on the possible presence of a vegetation cover (Arulanandan et al., 1980). F1

The aim of the present work is to set a rational framework relating the bankfull channel width and depth to the discharge flowing in the channel, to the longitudinal channel slope, to the median size of the sediment composing the channel bed, and to the resistance to erosion of the channel banks, assumed to be composed of cohesive material. This framework will be used to derive general relations valid for both gravel and sand rivers. We anticipate that the bankfull cross-sectional geometry of both types of rivers can be robustly described through a unique relationship if the skin friction shear stress responsible for bank erosion is properly accounted for. Specifically, as shown by Kean and Smith (2006a), the effective shear stress, that is, the shear stress actually acting on the bank surface, is controlled by the presence of bumps on the bank surface that determine the partitioning of the total shear stress into skin friction and drag resistance. Applying this partitioning, the equilibrium cross-section width is attained when the effective shear stress equals the critical threshold for particle erosion.

Figure 1. View of the Cecina River, near Casino di Terra (Pisa, Italy): (a) The river bed consists of gravel sediment, while the banks are composed of an upper cohesive layer and a basal layer of gravel, packed and slightly cemented with fine sediment, and are covered by loose material at the bank toe (Photo by Luca Solari); (b) the plan view shows clear evidence of erosion processes (flow from right to left, picture from Google Earth, acquisition 3 September 2017, geographical coordinate 43°19′33″ N 10°42′03″ E).

The paper is organized as follows. First, the model is formulated and applied to describe the widening of an initially narrow cross section until it reaches its equilibrium width. This procedure is then applied to a large data set of gravel and sand bed rivers to derive universal relationships (i.e., valid for gravel bed and sand bed rivers) for predicting the equilibrium width and depth of river cross section. Finally, a discussion section and some conclusion remarks close the paper.

2. Formulation of the Model

Our aim is to determine the equilibrium bankfull width of a single-thread channel with longitudinal slope S and median grain size D_{50} of the bed sediment. The channel is assumed to have a cross section that, as a first approximation, can be schematized as rectangular, with a top bankfull width B_{bf}. The coordinates normal to the channel bed and the banks are denoted with y and z, respectively (Figure 2a). F2

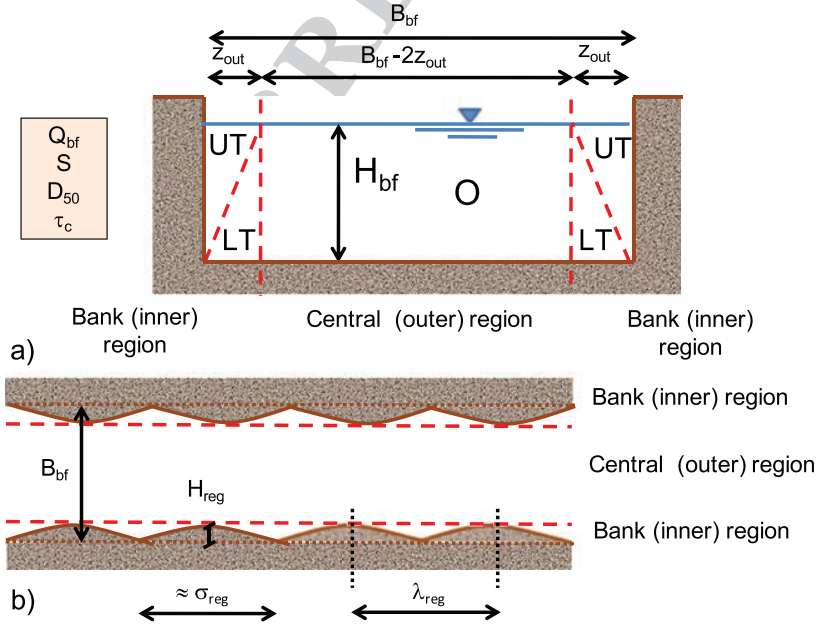

Figure 2. Definition sketch and notation. (a) Cross-section schematic: The labels denote the central region (O), the upper (UT), and the lower triangle (LT) near to the banks; (b) top view of a river reach with a regular sequence of equivalent Gaussian bumps along the banks. The relevant parameters controlling the in-channel flow are the bankfull flow discharge Q_{bf}, the longitudinal mean slope S, the median grain size of the channel bed D_{50}, and the critical shear stress for bank sediment erosion τ_c.

The bankfull flow, assumed to be uniform, conveys a discharge Q_{bf} with a bankfull flow depth H_{bf} and a cross-sectionally averaged velocity U_{bf}, such that

$$\frac{U_{bf}}{u_{*bf}} = \frac{C_{bf}}{g^{1/2}}, \qquad u_{*bf} = (g\ S\ R_{bf})^{1/2}, \tag{1}$$

with g acceleration of gravity, u_{*bf} friction velocity, R_{bf} hydraulic radius at bankfull conditions, and C_{bf} overall Chezy coefficient. This latter quantity depends on the different resistance to the flow exerted by the movable bed and the cohesive banks (Buffington and Montgomery, 1999). It is thus determined by partitioning the cross section in a rectangular central (core) region, of width $B_{bf} - 2z_{out}$, and two bank regions, of width equal to the thickness z_{out} of the boundary wall layer computed as

$$z_{out} = 2\frac{u_{*T}^2}{g\ S}, \tag{2}$$

where $u_{*T} = (\tau_T/\rho)^{1/2}$, with τ_T the total shear stress exerted on the banks.

The wall regions, in turn, are subdivided in two triangles of areas $H_{bf}\ z_{out}/2$ in which the flow resistance is dictated by channel bed roughness (low triangle) and bank roughness (upper triangle). We can then write

$$Q = A_{bf}\ U_{bf} = A_0\ U_0 + 2\ (A_{LT}\ U_{LT} + A_{UT}\ U_{UT}), \tag{3}$$

where the subscript 0 denotes the central region of the flow while the subscripts LT and UT denote the lower and upper triangles, respectively, by which each bank region has been decomposed (Figure 2) according to the method proposed by Marchi (1961) and Yen (2002). On the other hand, expressing the flow resistance in terms of the Chezy coefficients for the various flow regions, we can write

$$A_{bf}\ C_{bf}\ \sqrt{S\ R_{bf}} = A_0\ C_0 \sqrt{S\ R_0} + 2(A_{LT}\ C_{LT} \sqrt{S\ R_{LT}} + A_{UT}\ C_{UT} \sqrt{S\ R_{UT}}). \tag{4}$$

We eventually obtain

$$C_{bf} = \frac{C_0\ (B_{bf} - 2\ z_{out}) + \left[C_{LT}\ z_{out} + C_{UT}\ (z_{out}/H_{bf})^{3/2}\ H_{bf}\right]/\sqrt{2}}{B_{bf}\ (1 + 2H_{bf}/B_{bf})^{-1/2}}. \tag{5}$$

In the central region of the flow, the velocity profile in the direction y normal to the bed can be expressed as

$$u(y) = \frac{u_{*0}}{\kappa}\ \ln\left(\frac{y}{y_{0T}}\right), \tag{6}$$

with κ (= 0.4) the von Karman constant, $u_{*0} = (\tau_0/\rho)^{1/2}$ the friction velocity related to the total shear stress τ_0, and $y_{0T} = 0.033\ e_s$ a reference level where the velocity vanishes, related to the effective roughness height e_s on the basis of experimental data (van Rijn, 1984). The mean flow velocity U_0, the friction velocity u_{*0}, and the Chezy coefficient C_0 can then be computed as

$$U_0 = \frac{C_0}{\sqrt{g}}\ u_{*0}, \qquad u_{*0} = \sqrt{g\ S\ H_{bf}}, \qquad \frac{C_0}{\sqrt{g}} = 18\ \log\left(\frac{12\ H_{bf}}{e_s}\right), \tag{7}$$

where, following van Rijn (1984), the effective roughness e_s is set equal to 3 D_{90} in the case of a plane bed (with D_{90} the grain diameter such that 90% of the material is finer) or

$$e_s = 3\ D_{90} + 1.1\ A_d\ \left(1 - e^{A_d/\lambda_d}\right) \tag{8}$$

in the case of a bed covered by dunes of amplitude A_d and wavelength λ_d, with

$$\frac{A_d}{\lambda_d} = 0.015 \left(\frac{D_{50}}{H_{bf}}\right)^{0.3} \left(1 - e^{0.5\ T}\right)(25 - T), \qquad \lambda = 7.3\ H_{bf}. \tag{9}$$

Here, $T = (u'_{*0} - u_{*c})/u_{*c}$ is the transport stage parameter, computed on the basis of the critical bed shear velocity u_{*c} for incipient sediment movement according to shields and of the bed shear velocity u'_{*0} related to grain roughness:

$$u'_{*0} = \frac{\sqrt{g}}{C_{90}}\ U_0, \qquad \frac{C_{90}}{\sqrt{g}} = 18\ \log\left(\frac{12\ H_{bf}}{3\ D_{90}}\right). \tag{10}$$

As far as the bank regions are concerned, field observations (Kean and Smith, 2006a, 2006b) indicate that usually, the bank surface is characterized by macroscopic undulations (Figure 2b); here denoted as bumps, caused by processes such as erosion, slumping of bank material and vegetation encroachment. The flow near each bank is strongly modulated by the presence of these undulations. Similarly to bedforms that develop on the channel bed (dunes), these macroroughness elements generate a form drag due to the overall unbalance of pressures acting on the upstream and downstream side of each bump. The sum of the shear stress τ_d associated with form drag and the skin friction τ_{sf} due to the grain roughness of the material composing the banks yield the total shear stress (Kean and Smith, 2006a):

$$\tau_T = \tau_{sf} + \tau_d. \tag{11}$$

Under equilibrium conditions, the diffusion of momentum toward the bank is needed to compensate the losses due to form drag and skin friction on the bumps, and it produces in the bank boundary layers a logarithmic velocity profile of the form

$$u(z) = \frac{u_{*T}}{\kappa} \ln\left(\frac{z}{z_{0T}}\right), \tag{12}$$

with $u_{*T} = (\tau_T/\rho)^{1/2}$ and z_{0T} the roughness height due to the sum of skin friction and form drag resulting from (Kean and Smith, 2006a) analysis (see Appendix A).

The mean velocities in the lower and upper triangles near to the banks can then be computed as

$$U_{LT} = \frac{u_{*0}}{H_{bf}\ z_{out}/2} \int_{z_{0T}}^{z_{out}} d\,z \int_{y_{0T}}^{z\ H_{bf}/z_{out}} \frac{1}{\kappa} \ln\left(\frac{y}{y_{0T}}\right)\, dy, \tag{13}$$

$$U_{UT} = \frac{u_{*T}}{H_{bf}\ z_{out}/2} \int_{y_{0T}}^{H_{bf}} d\,y \int_{z_{0T}}^{y\ z_{out}/H_{bf}} \frac{1}{\kappa} \ln\left(\frac{z}{z_{0T}}\right)\, dz. \tag{14}$$

The integrals into equations (13) and (14) can be easily solved to yield

$$\frac{C_{LT}}{\sqrt{g}} = \frac{1}{\kappa}\left[\ln\left(\frac{H_{bf}}{y_{0T}}\right) - \frac{3}{2} + 2\,\frac{y_{0T}}{H_{bf}} - \left(\frac{z_{0T}}{z_{out}}\right)^2 \ln\left(\frac{z_{0T}\ H_{bf}}{z_{out}\ y_{0T}}\right) + \frac{3}{2}\left(\frac{z_{0T}}{z_{out}}\right)^2 - \frac{2\ z_{0T}\ y_{0T}}{z_{out}\ H_{bf}}\right], \tag{15}$$

$$\frac{C_{UT}}{\sqrt{g}} = \frac{1}{\kappa}\left[\ln\left(\frac{z_{out}}{z_{0T}}\right) - \frac{3}{2} + 2\,\frac{z_{0T}}{z_{out}} - \left(\frac{y_{0T}}{H_{bf}}\right)^2 \ln\left(\frac{y_{0T}\ z_{out}}{H_{bf}\ z_{0T}}\right) + \frac{3}{2}\left(\frac{y_{0T}}{H_{bf}}\right)^2 - \frac{2\ z_{0T}\ y_{0T}}{z_{out}\ H_{bf}}\right]. \tag{16}$$

It is worthwhile to observe that, according to the procedure developed by (Kean and Smith, 2006a), the overall shear stress τ_T exerted on the banks can be expressed in terms of a specified outer velocity U_{out}. In the present case, it can be reasonably assumed that the relevant outer velocity is equal to the mean velocity along the hypotenuse of each of the lower triangles located near to the banks. Under this assumption, it can be demonstrated that $U_{out} = U_0$ and setting $z = z_{out}$ in equation (12) so that:

$$u_{*T} = \frac{\kappa\ U_0}{\ln\left(z_{out}/z_{0T}\right)}. \tag{17}$$

The decomposition (11) of the bank shear stress is crucial for estimating river bank erosion. Indeed, although the form drag stress τ_d is typically the larger component (Darby et al., 2010; Thorne and Furbish, 1995), only the skin component τ_{sf} is responsible for sediment particle erosion (Smith and McLean, 1977). As a consequence, we expect that the equilibrium channel width is much smaller than that obtained by requiring that the total shear stress τ_T should be at a maximum equal to the critical shear stress τ_c for particle erosion.

In the following, we will use τ_{sf} to drive bank erosion and to eventually compute the channel width B_{eq} for which the bankfull discharge Q_{bf} flows with a depth H_{bf}. Starting from an initial relatively narrow section of width B_0, the cross section is allowed to widen because of bank erosion, until an equilibrium width B is attained for $\tau_{sf} = \tau_c$.

Clearly, many different processes are involved in bank erosion and hence to determine the equilibrium width. In particular, bank shear stress is highly variable both in space and time, depending on bank geometry, cross-section size and shape, channel axis curvature, and flow stage. This variability makes it quite difficult to determine direct estimates of the along bank shear stress distribution and, as a consequence, the quantification of bank retreat. In addition, erosion of river banks includes a number of mechanisms due to both the shear stress exerted by the flow (e.g., weathering of the bank material and direct removal either of individual grains or as layers; Papanicolaou et al., 2017) and gravitational processes (e.g., mass wasting triggered by erosion of the bank toe material; Amiri-Tokaldany et al., 2003). In the present approach, all these erosion processes are assumed to give rise to an average erosion rate, depending on the excess of τ_{sf} with respect to τ_c. Specifically, we write (e.g. Partheniades, 1965)

$$\epsilon = k\,\left(\tau_{sf} - \tau_c\right)^{\alpha}, \tag{18}$$

where ϵ (m/s) is the rate of fluvial bank erosion per unit time and unit area, k (m^2s/kg) is the bank erodibility coefficient, and α (dimensionless) is an empirical exponent, often approximated as 1 (Rinaldi and Darby, 2007).

2.1. Critical Shear Stress and Erodibility of the Bank

The critical shear stress for bank erosion τ_c is a key factor in the present approach. Nevertheless, its estimate is usually uncertain and time consuming, owing to its variability along the banks and the coexistence of various mechanisms that drive river-bank erosion and mass failure (Rinaldi and Darby, 2007). In addition, several other factors can matter, such as clay and organic content, and the composition of interstitial fluids (Arulanandan et al., 1980; Grissinger, 1982).

In the absence of direct measurements, the erodibility parameters k and τ_c typical of riverbank materials are often estimated indirectly through calibration of equation (18) (Julian and Torres, 2006) or by using laboratory flumes (Jepsen et al., 2010; Sutarto et al., 2014). On the other hand, detailed measurements of (k, τ_c) are rare in the literature. These measures are in fact time and resource consuming and still present a variety of limitations. In particular, the heterogeneity of cohesive materials (Arulanandan et al., 1980; Grissinger, 1982; Samadi et al., 2009) and the high variability of the critical shear stress along the bank profile (Papanicolaou et al., 2007, 2017; Sutarto et al., 2014) impose repeated sampling for an accurate description of erosion properties. In addition, the presence of vegetation can alter or invalidate the measurements, especially when varying seasonally during the year. Generally, direct estimates of k and τ_c can be obtained by means of in situ jet tests based on measured deformation rate, scour depth, and known hydraulic properties (Hanson and Simon, 2001). Alternatively, τ_c can be estimated through cohesive strength meter (CSM) measurements (see, e.g., Darby et al., 2010; Nardi and Rinaldi, 2010), based on the reduction of the optical transmission in the sampling head chamber due to suspension of eroded sediment (Tolhurst et al., 1999). The bank erodibility k, not provided by CSM measurements, can be estimated using an empirical relationship whereby k is strongly related to $\tau_c^{-0.5}$ (Darby et al., 2010). Anyhow, we note that, for our aims, the value of k is likely to affect the time a cross-section takes to widens up to equilibrium and not the equilibrium width. Hence, in the following, as a first step toward the testing of the proposed modeling framework, we will set $k = 1 m^2 s/kg$ on the basis of Rinaldi and Darby (2007) suggestion.

2.2. Bump Metrics

Even though the spatial distribution on the banks of macroroughnesses is in general irregular, a systematic series of tests, carried out with different combinations of four types of bumps, indicated a relatively small variability of the average bank shear stress with respect to the relative size and the relative position of the undulations (Kean and Smith, 2006b). The overall effect of an irregular sequence of bumps can then be reproduced by considering an equivalent Gaussian bump shape (Kean and Smith, 2006b), hereafter denoted as regular (i.e., identified with the subfix $_{reg}$). This equivalent geometry produces the same spatially averaged flow velocity and is described by means of geometric parameters such as the protrusion height of the equivalent element, H_{reg}; the spacing of elements, λ_{reg}; and the streamwise length scale of elements, σ_{reg}, defined as

$$H_{reg} = H_{88}, \qquad \sigma_{reg} = \sigma_{88}, \qquad \lambda_{reg} = 6\,H_{88}, \tag{19}$$

with H_{88} and σ_{88} the 88^{th} percentiles of the spatial distributions of H and σ for the irregular bump sequence to be approximated (Kean and Smith, 2006b).

Table 1
Bumps Metrics and Hydraulic Variables Measured in Various Rivers

Location	H_{reg} [m]	σ_{reg} [m]	λ_{reg} [m]	Q_{bf} [m^3/s]	S [$-$]	D_{50} [mm]	H_{bf} [m]	B_{bf} [m]
Lost Creek	0.173	0.120	1.035	5	0.015	8.0	1.0	4.5
Rock Creek	0.082	0.168	0.492	20	0.015	8.0	1.6	8.8
Whitewater River	0.487	1.979	2.923	170	0.005	8.0	5.5	33
Cecina River	0.1621	0.9915	*n.a.*	140	0.002	7.4	2.3	70
Mekong River, Ang Nyay	2.37	6.55	14.22	16750	$1.0 \cdot 10^{-4}$	*n.a.*	≈ 13	$800 - 1300$
Mekong River, Ban Hom	1.82	4.14	10.91	16750	$1.0 \cdot 10^{-4}$	*n.a.*	≈ 13	$800 - 1300$
Mekong River, Friendship Bridge	1.33	2.62	7.99	16750	$1.0 \cdot 10^{-4}$	*n.a.*	≈ 13	$800 - 1300$
Mekong River, Pakse	3.81	5.1	22.86	37700	$6.0 \cdot 10^{-5}$	*n.a.*	≈ 13	≈ 2000

Note. Sources are as follows: Lost Creek, Rock Creek, and Whitewater River, Kean and Smith (2006a); Cecina River, Nardi and Rinaldi (2010); Mekong River, Darby et al. (2010). "n.a." stands for not available..

Figure 2 shows a sketch of a typical cross section and a schematic top view of a river reach with Gaussian-like macroroughness elements along both banks, while Table 1 summarizes some published data of equivalent bump geometry, together with the corresponding hydraulic variables. The data, derived from field measurements of the actual irregular geometry, suggest that bump metrics scale with the hydraulic characteristics of the considered river. In general, wider rivers have bigger roughness elements, as shown in Figure 3a, using the data of Table 1 for H_{reg} and B_{bf}. On the other hand, Figure 3b shows that bump height scales with the element length. Hence, owing to the Gaussian-shape used to approximate the observed irregular bump geometry, only one parameter (e.g., H_{reg}) is sufficient to describe the equivalent bump geometry.

Finally, it is worthwhile to observe that bump geometry can vary with the flow discharge (Leyland et al., 2015). Periods of intense erosion, usually associated with large flood events, lead to an increase of the riverbank macroroughness. This increase, however, enhances the thickness of the near-bank boundary layer and, consequently, decreases the skin friction responsible for bank erosion, implying a negative feedback mechanism that leads to a smoothing of bump induced roughness and, on average, to an almost constant geometry of the bumps.

3. Modeling Cross-Section Widening

The modeling framework described so far is here used to predict the equilibrium width of rivers with cohesive banks. The overall structure of the Cross-Section Evolution Model (CSEM) is described in Figure 4. The model consists of three main units: the flow unit, which computes the flow variables in the central channel region; the Kean and Smith unit, which solves the flow close to the bank region; and the erosion unit, which predicts the rate of riverbank erosion.

The solution is based on an iterative, three-step procedure that, starting from an initial narrow cross section, allows the section to widen while conserving the subvertical bank shape (see, e.g., Figure 1a), until it reaches

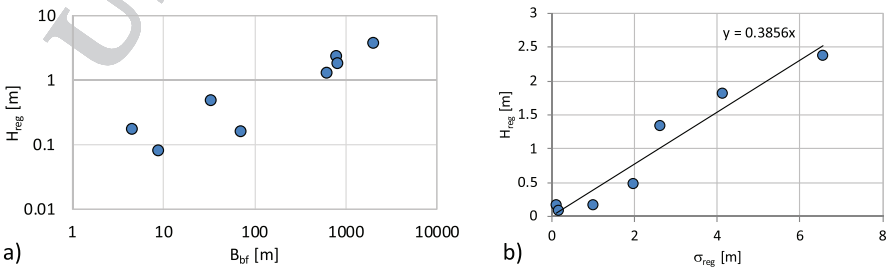

Figure 3. Relationship between (a) equivalent bump height, H_{reg}, and bankfull channel width, B_{bf}; (b) equivalent bump height, H_{reg}, and equivalent bump length, σ_{reg}, for the river data reported in Table 1 (coefficient of correlation for linear regression: $R^2 = 0.94$).

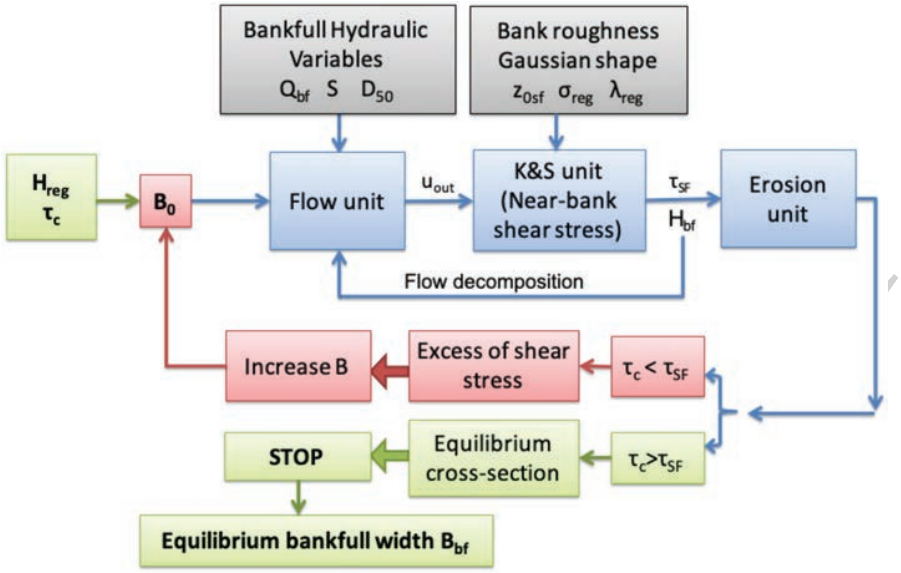

Figure 4. Overall structure of the CSEM model and iterative procedure used to determine the equilibrium cross-section width. The colors of the boxes refer to as follows: gray, input variables; blue, fundamental model units; red, options checked for river widening; and green, options checked for selecting the equilibrium bankfull width.

its equilibrium width. Given the bankfull discharge Q_{bf}, the channel slope S, the median grain size D_{50} of the sediment bed, and a trial value of the bankfull width, B_0, the model iteratively uses equations (2), (7), (15), and (16) to compute, through equations (1) and (3), the actual value of H_{bf}. The values of z_{0T} and τ_{0T} needed for these computations are obtained from the Kean and Smith unit, which also provides the skin friction shear stress, τ_{sf}. This value is subsequently used in the erosion unit. If $\tau_{sf} > \tau_c$, the river widens according to equation (18), and the iterative procedure starts again with an increased value of width $B > B_0$. Otherwise, if $\tau_{sf} < \tau_c$, the cross section is assumed at equilibrium, and the algorithm stops, giving the equilibrium bankfull width B_{bf}. Note that the narrowing process is not considered in the model.

Table 2
Databases Used in Conjunction With the CSEM Model to Derive Universal Relationships for Equilibrium Cross Section

Database	*Source*	*Code (Number of selected data)*	*River type*
1	Soar and Thorne (2001)	*ST*(55)	Sand
	Mc Candless (2003b)	*MCC*(12)	Sand and Gravel
	Metcalf (2004)	*MET*(13)	Sand
	Mistak and Stille (2008)	*MS*(2)	Sand
	Mulvihill et al. (2005)	*MUL*1(11)	Sand and Gravel
	Mulvihill et al. (2006)	*MUL*2(8)	Sand and Gravel
	Sherwood and Huitger (2005)	*SH*(14)	Sand and Gravel
	Agourdis et al. (2011)	*AGO*(15)	Gravel
	Chaplin (2005)	*CHA*(43)	Gravel
2	Chitale (1970, 1973)	*CC*(21)	Sand
	Roth (1985)	*RSH*(2)	Sand
3	Hey and Thorne (1986)	*HT*(55)	Gravel
4	Church and Rood (1983)	*CR*(11)	Sand
5	Cecina River	*C*(1)	Gravel

Note. (1) Trampush et al. (2014); (2) Li et al. (2015); (3) Hey and Thorne (1986); (4) Wilkerson and Parker (2011); (5) Nardi and Rinaldi (2010).

Table 3
Databases Used in Conjunction With the CSEM Model to Validate Universal Relationships for Equilibrium Cross Section

Database	*Source*	*Code (Number of selected data)*	*River type*	*Notes*
1	Cinotto (2003)	*CIN*(8)	Gravel	Pennsylvania, USA
	Keaton et al. (2005)	*KEA*(38)	Gravel	$B < 5$ m not used
	Lawlor (2004)	*LAW*(27)	Gravel	$B < 5$ m not used
2	Annable (1996)	*ANN*(3)	Sand	Southern Ontario, CAN
	Loell Duell (2006, unpubl.)	*DUE*(4)	Sand	Oregon, USA
	Charlton et al. (1978)	*CBB*(23)	Gravel	Great Britain
	Kellerhals et al. (1972)	*KNB*(16)	Gravel	Alberta, CAN
	Schumm (1960)	*SCH*1(11)	Sand	Central USA
	Schumm (1968)	*SCH*2(8)	Sand	Australia
	Parker et al. (2003)	*PTRB*(23)	Gravel	Idaho, USA
	Vermont DEC (2006)	*VTDEC*(7)	Transitional	Vermont, USA
	Pitlick and Cress (2000)	*PC*(10)	Gravel	Colorado, USA
	William (1978)	*WIL*(1)	Sand	New Mexico, USA
	Westergard et al. (2005)	*WMEB*(2)	Sand	New York, USA
3	Lagasse et al. (2004)	*LAG*(69)	Sand and Gravel	Meander rivers, USA
4	Andrews (1984)	*COL*(24)	Gravel	Colorado, USA

Note. (1) Trampush et al. (2014); (2) Li et al. (2015); (3) Lagasse et al. (2004); (4) Andrews (1984).

The quantities characterizing the Gaussian-shaped bank geometry (H_{reg}) and the bank erodibility (τ_c) can be treated either as input data for the model (when known from direct measurements) or as input parameters when the model is used for predicting the equilibrium channel width. In this latter case, the H_{reg} and τ_c are calibration parameters that are adjusted to obtain the best agreement between computed and observed bankfull width, B_{bf}. In particular, following the works of Arulanandan et al. (1980), Darby et al. (2010), Nardi and Rinaldi (2010), Sutarto et al. (2014), Papanicolaou et al. (2017), we assume that, in the absence of vegetation, a reasonable range of variation for τ_c is 0.5–4 Pa, while in the presence of vegetated banks τ_c can increase by up to a factor of 2.5 for high vegetation density (see, e.g., Figure 8 from Parker et al., 2007).

3.1. Considered Data Sets

Two independent data sets have been used for testing and validating the CSEM model. They were extracted from previous studies on channel bank properties (Nardi and Rinaldi, 2010) and from available databases providing the bankfull characteristics of alluvial channels (Lagasse et al., 2004; Li et al., 2015; Trampush et al., 2014; Wilkerson and Parker, 2011). The list of data considered to develop the model is summarized in Table 2, while Table 3 refers to the data used in the model validation. Both tables provide some basic information on the original source, the number of data, and the type of river (sand or gravel) they refer to. For a given river, the data consist of bankfull discharge Q_{bf}, bankfull depth H_{bf}, bankfull width B_{bf}, reach slope S, and median sediment size D_{50} of the bed.

A number of criteria were considered to choose data appropriate for the requirements of the model among the whole available data set. First of all, the considered river should have cohesive river banks. When geographical coordinates were available (for 119 records of the total), we verified on Google Earth the planimetric river pattern, the structure of the banks, and the possible presence of vegetation over the banks. Second, the Shields number calculated at bankfull condition,

$$\hat{\tau}_{bf} = \frac{\rho S\, H_{bf}}{(\rho_s - \rho)\, D_{50}}, \tag{20}$$

(with ρ_s and ρ the density of sediment and water, respectively) was verified to ensure sediment transport (Figure 5a). Third, the Froude number at bankfull conditions,

$$Fr = \frac{Q_{bf}}{H_{bf}\, B_{bf}} \frac{1}{\sqrt{g\, H_{bf}}}, \tag{21}$$

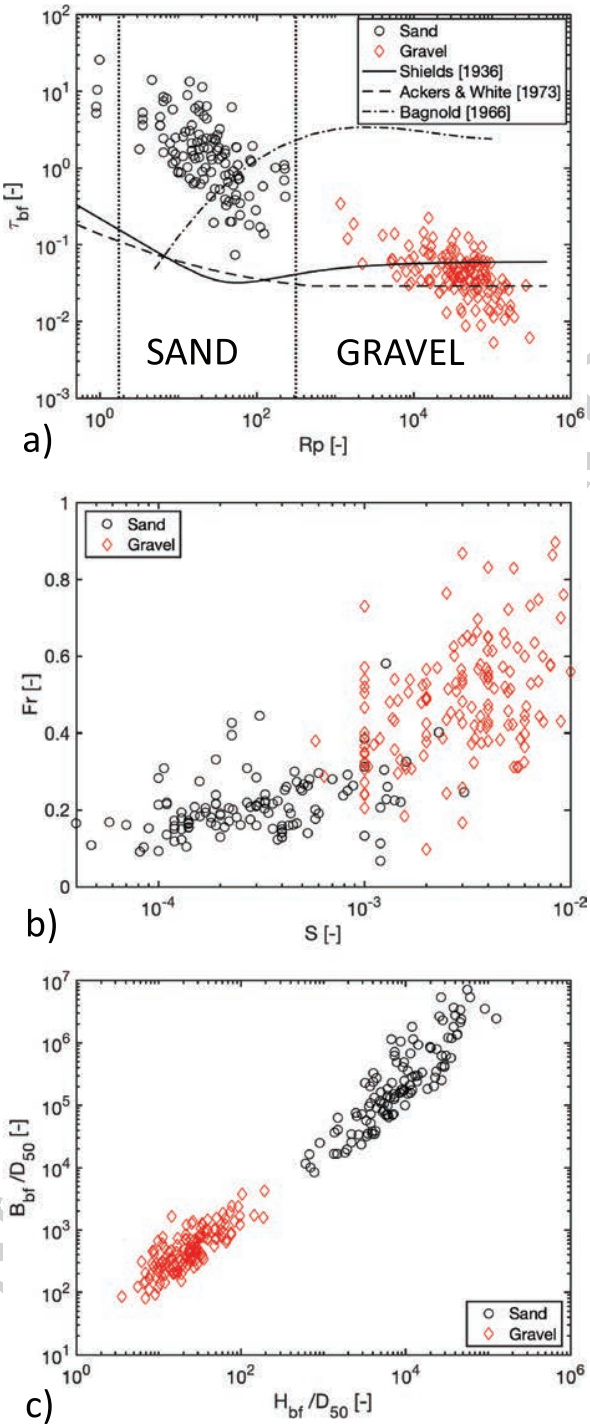

Figure 5. (a) The bankfull Shields number, τ^*_{bf}, is plotted versus the particle Reynolds number $R_p = (\Delta g D^3)^{0.5}/\nu$ (with Δ the immersed relative density and g gravity constant). The black vertical lines represent the limits between silt and sand fractions ($D = 0.0625$ mm) and between sand and gravel fractions ($D = 2$ mm). The solid line denotes the empirical threshold for incipient sediment motion derived by Shields (1936), while the dashed line represents the relation by Ackers and White (1973). The point-dashed line denotes the condition for incipient suspended load proposed by Bagnold (1966). (b) The Froude number, Fr, is plotted versus the channel slope, S. (c) Relationship between the bankfull channel width, B_{bf}, and flow depth, H_{bf}, both scaled by the mean grain size, D_{50}. Data are those extracted from the database reported in Table 2.

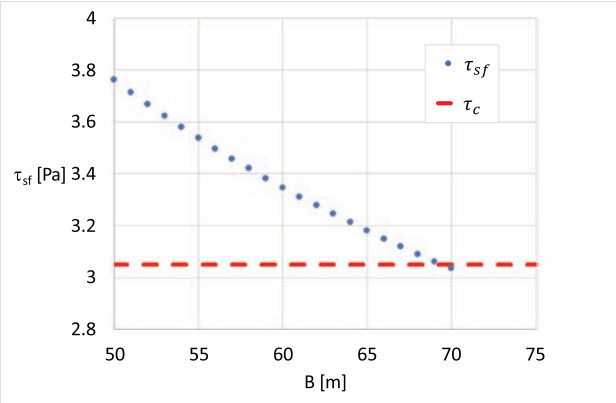

Figure 6. Simulation obtained with the CSEM model applied to the Cecina River case study. Starting from a narrow section of width B_0, the bankfull width decreases until the skin friction shear stress at the bank τ_{sf} is below the critical value τ_c for bank erosion.

was verified to be in the subcritical range, in order to satisfy the conditions for applying the Kean and Smith (2006a) model (Figure 5b). For similar reasons, records with bed slope higher than 0.01 were removed, to guarantee subcritical flow. Finally, records with flow discharge below 1 m^3/s and width to depth ratio smaller than 8 were disregarded. This latter choice is related to the need that the bank boundary layer does not occupy the central flow region.

Before proceeding further, some comments on the considered data are worthwhile. The Shields stresses reported in Figure 5a indicate that, for bankfull flow conditions, sandy rivers generally keep well above the threshold for incipient motion, such that in many cases sediments are transported not only as bedload but also as suspended load. Conversely, gravel-bed rivers are close to the threshold for incipient sediment motion, and, consequently, sediments are transported as bedload (e.g., Buffington 2012; Dade and Friend, 1998; Garcia, 2000). Sandy rivers invariably exhibit subcritical flow conditions, while gravel-bed rivers tend toward supercritical flow conditions for high enough slopes (Figure 5b). Finally, when made dimensionless with the mean bed sediment diameter D_{50}, the relationship between river width and water depth at bankfull conditions tends to follow an almost universal trend, both for gravel and sand rivers (Figure 5c).

3.2. Example of Model Application

In order to clarify the CSEM procedure, in this section we describe its application to the Cecina River (Italy). The main hydraulic variables for this river are $Q_{bf} = 75$ m^3/s, $S = 0.002$, $D_{50} = 0.0038$ m, $H_{bf} = 2.3$ m, and $B_{bf} = 70$ m (Nardi and Rinaldi, 2010). As already reported in section 1, Cecina River has composite cohesive banks, and the value of τ_c for the sandy layers was around 1.25 Pa, while the average value for the whole bank to be assumed for fluvial erosion can be up to 2.5–3 times higher. For these reasons, the spanning input values for τ_c were in the range 1.0–3.1 Pa. Moreover, in the Cecina River the existing measurements of bump geometry (Leyland et al., 2015; Nardi and Rinaldi, 2010) helped us to define a spanning interval for $H_{reg} = 0.08$–0.4 m. The values of σ_{ref} and λ_{reg} are estimated on the basis of bump shape and metric relationships described in section 2.2. For each combination of (τ_c, H_{reg}), the equilibrium value of B_{bf} was choosen among all the possible solutions as that minimizing the error between B_{bf} calculated and B_{bf} measured. The goal here was to verify that the CSE Model is able to predict the measured value of bump geometry when equilibrium bankfull width is attained. We thus run the CSE Model using as input data the hydraulic variables reported above, as well as H_{reg} and τ_c (see Figure 6, green box) and an initial width of $B_0 = 50$ m. The values of H_{reg} and τ_c were selected spanning their physically admissible ranges, and the computed equilibrium widths yielded a surface $B_{bf}(H_{reg}, \tau_c)$ in the three-dimensional space $(H_{reg}, \tau_c, B_{bf})$. The couple of values (τ_c, H_{reg}) providing the best fitting was chosen as that ensuring the minimum distance between this surface and the plane $B_{bf} = B_{bf}^{observed}$ representing the observed channel width.

The results of the simulation ensuring the best fit are shown in Figure 6. The river cross-section widens progressively until the skin friction shear stress at the bank falls below the threshold for bank erosion. The observed equilibrium width ($B = 70$ m) is obtained for $H_{reg} = 0.16$ m and $\tau_c = 3.05$ Pa: H_{reg} is in excellent agreement with measured data (see Table 1), while τ_c is in the range of admissible values.

4. Results

The CSE Model has been first used in conjunction with the data of Table 2 to derive suitable relations that express the bump height and the critical shear stress for bank erosion. Next, these relations are used to relate the dimensionless bankfull depth and width to the dimensionless flow discharge. Finally, these latter relations have been validated by using the independent set of data reported in Table 3.

4.1. Universal Relationships for Equilibrium Cross Section

The data set used to obtain the dimensionless relations giving H_{reg} and τ_c as a function of Q_{bf} is that reported in Table 2 and is composed by 263 records. For each river, given the observed values of the hydraulic variables

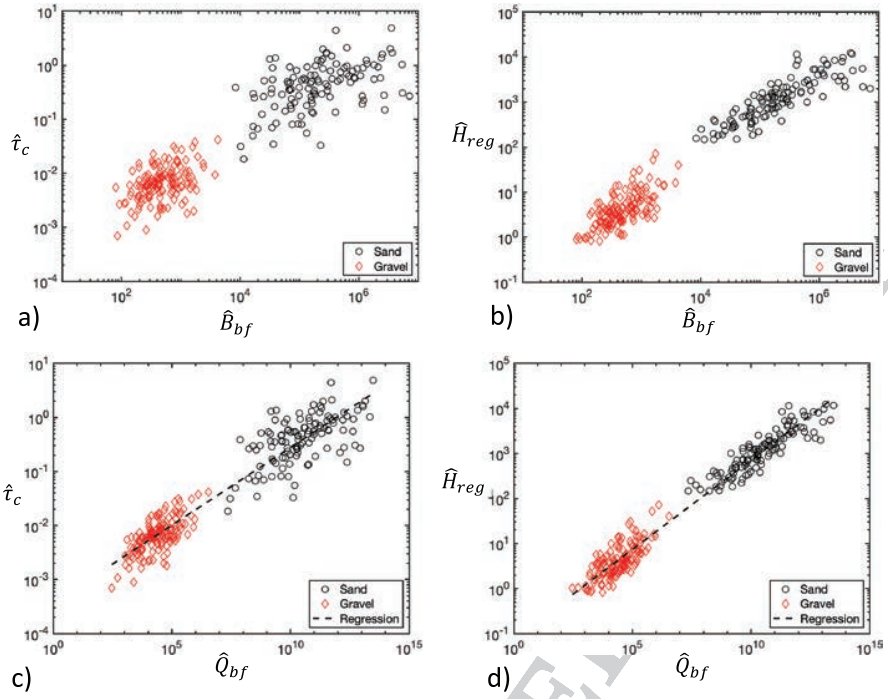

Figure 7. The dimensionless critical stress for bank erosion, $\hat{\tau}_c$, and the mean bump height, $\hat{H}_{reg}$, predicted through the CSE Model are plotted versus (a and b) the dimensionless channel width at bankfull discharge, $\hat{B}_{bf}$ and (c and d) the dimensionless bankfull discharge, $\hat{Q}_{bf}$. The regression curves for panels c and d are reported in equations (23)–(24).

(Q_{bf}, S) and of the median diameter D_{50} of the sediment bed, the parameters τ_c and H_{reg} are both varied until the bankfull width predicted by the model differs with respect to that observed in the field by a prescribed tolerance (on average 2–3%, maximum 5%). The results of this analysis are shown in Figure 7 in terms of the dimensionless quantities: F7

$$\hat{\tau}_c = \frac{\tau_c}{(\rho_s - \rho)\, g\, D_{50}}, \qquad \hat{H}_{reg} = \frac{H_{reg}}{D_{50}}, \qquad \hat{B}_{bf} = \frac{B_{bf}}{D_{50}}, \qquad \hat{Q}_{bf} = \frac{Q_{bf}}{\sqrt{g\, D_{50}^5}}. \tag{22}$$

The quantities $\hat{\tau}_c$ and $\hat{H}_{reg}$ appear to be poorly related to the dimensionless bankfull width $\hat{B}_{bf}$ (Figures 7a and 7b), with data corresponding to gravel and sand that cluster in two separate regions of the plot. Indeed, the power law regression relationships for $\hat{\tau}_c - \hat{B}_{bf}$ exhibit relatively low values of the coefficient of correlation for both sand-bed rivers ($R^2 = 0.24$) and gravel-bed rivers ($R^2 = 0.19$). Better correlations are attained by the regression $\hat{H}_{reg} - \hat{B}_{bf}$ yielding $R^2 = 0.74$ for sand-bed rivers and $R^2 = 0.46$ for gravel-bed rivers.

On the other hand, Figures 7c and 7d show that $\hat{\tau}_c$ and $\hat{H}_{reg}$ are strongly related to the dimensionless bankfull discharge $\hat{Q}_{bf}$ through a power law that seems to be universal for sand-bed and gravel-bed rivers. The corresponding regression curves are as follows:

$$\hat{\tau}_c = 0.0003679\ \hat{Q}_{bf}^{0.2878} \quad (R^2 = 0.903), \tag{23}$$

$$\hat{H}_{reg} = 0.0768\ \hat{Q}_{bf}^{0.3967}, \quad (R^2 = 0.965). \tag{24}$$

Given the high values of coefficient of variation R^2, these relations provide robust estimates of the representative bump height, H_{reg}, and of the critical shear stress for bank erosion, τ_c, given the bankfull discharge Q_{bf} and the bed sediment diameter, D_{50}.

In the absence of any information based on field observations, these values of H_{reg} and τ_c can be used to relate to the bankfull discharge other quantities such as the bankfull flow depth and width. For this purpose, we

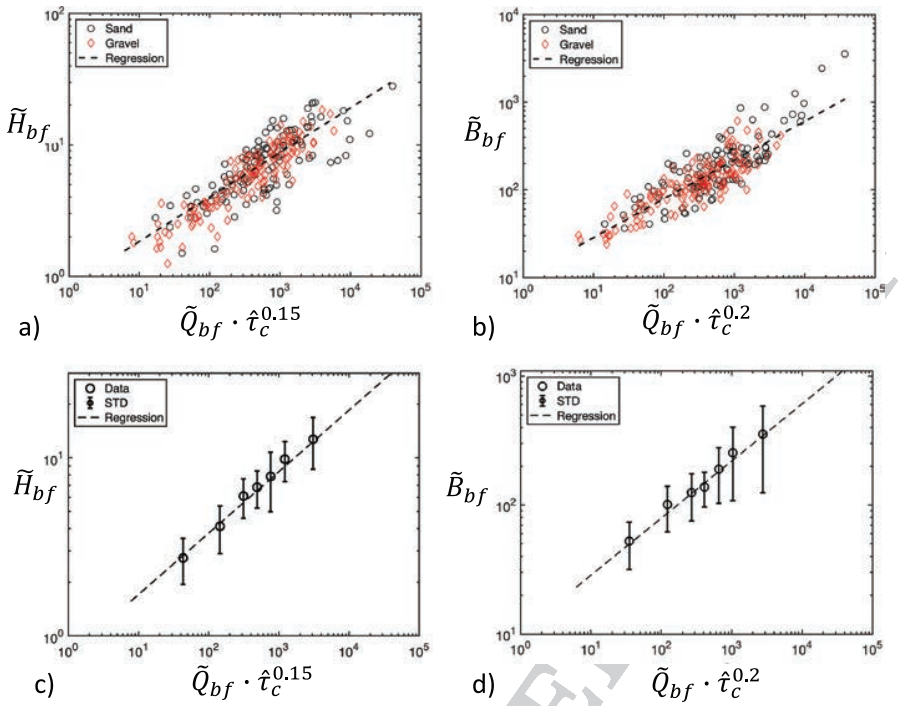

Figure 8. Determination of universal relationships for equilibrium conditions of river cross section as a function of the dimensionless bankfull discharge $\tilde{Q}_{bf}$ and the dimensionless critical stress τ_c. (a and c) Dimensionless bankfull depth, $\tilde{H}_{bf}$, scaled with H_{reg} ($R^2 = 0.733$); (b and d) dimensionless bankfull width, $\tilde{B}_{bf}$, scaled with H_{reg} ($R^2 = 0.723$). The plots c and d have been obtained by considering an uniform binning of the data, each bin containing 37 data; vertical lines denote the standard error with respect to the mean within a bin.

use the bump height H_{reg} as a characteristic length scale and introduce three new dimensionless variables:

$$\tilde{H} = \frac{H_{bf}}{H_{reg}}, \qquad \tilde{Q} = \frac{Q_{bf}}{\sqrt{g\, H_{reg}}\, H_{reg}^2}, \qquad \tilde{B} = \frac{B_{bf}}{H_{reg}}. \tag{25}$$

As shown in Figures 8a and 8b, this scaling suggests a power law dependence of the form F8

$$\tilde{H} = 0.7685 \left(\tilde{Q}\, \hat{\tau}_c^{0.15}\right)^{0.3456} \quad (R^2 = 0.73), \tag{26}$$

$$\tilde{B} = 10.294 \left(\tilde{Q}\, \hat{\tau}_c^{0.20}\right)^{0.4429} \quad (R^2 = 0.73). \tag{27}$$

These latter relationships exhibit a reasonable degree of correlation as also emerges from the binned plots shown in Figures 8c and 8d. In the absence of data, relations (26)–(27) can be used to predict the water depth and the equilibrium cross-section width, on the basis of the bankfull discharge, Q_{bf}, and the parameters τ_c and H_{reg}. These two quantities, in turn, can be either known directly from field measurements or determined through equations (23)–(24), requiring, besides Q_{bf}, knowledge of the median sediment grain size D_{50}. It is important to note that the whole data set, composed of either sand-bed and gravel-bed rivers, tends to collapse on a universal relationship, valid for equilibrium cross section with cohesive banks. This overlapping results from the inclusion of $\hat{\tau}_c$ into (26)–(27), to account for the properties of bank sediment (through τ_c) and of the bed (through D_{50}). Hereafter, following (Parker et al., 2007) and (Wilkerson and Parker, 2011), we denote as *universal* relationships (26)–(27).

4.2. Independent Test of Universal Relationships for Equilibrium Cross Section

The universal relationships determined in the previous section can be used to predict river width or water depth in rivers were only flow discharge and median size of the bed sediment are known. The relationships can also be used to assess how far away the river width is from equilibrium conditions. To address this aim, we tested relationships (26)–(27) by means of the completely independent set of data reported in Table 3.

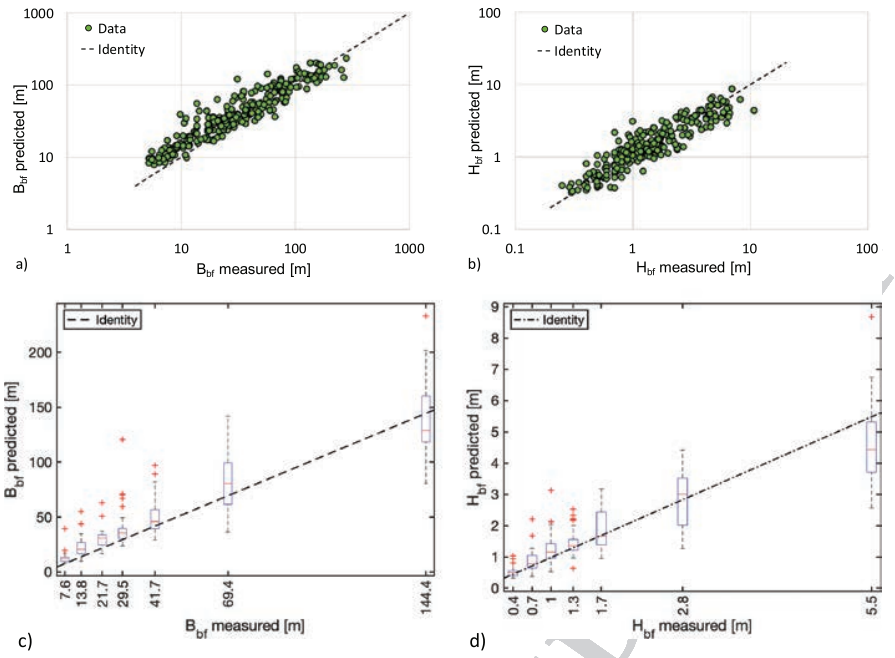

Figure 9. Validation of universal relationships (26)–(27) for equilibrium conditions of river cross section. (a) Predicted versus measured bankfull width. (b) Predicted versus measured bankfull depth. (c and d) Box plots of a and b with constant number of 39 samples for each box. Dashed lines denote the perfect agreement.

Figure 9 shows the comparisons between the values of H_{bf} and B_{bf} predicted by (26)–(27) and those measured in the field. In order to evaluate the model robustness, we calculated the coefficient of determination R^2, the index of agreement I_a, and the Nash-Sutcliffe Efficiency *NSE* (Nash and Sutcliffe, 1970). All these three statistical indexes provide a measure of how well observed data are replicated by the model. The closer these coefficients are to 1, the more accurate the model is, the value 1 corresponding to a perfect match of modeled observed data. In the case of the river width (Figure 9a) these statistical parameters take the values $R^2 = 0.78$, $I_a = 0.94$, and $NSE = 0.77$, while for river depth (Figure 9b) the values are $R^2 = 0.77$, $I_a = 0.93$, and $NSE = 0.77$. The overall agreement is reasonably good, for both the bankfull flow depth and width. In particular, the box plots shown in Figures 9c and 9d suggest that outliers are distributed at lower values of width and depth, leading to possible overestimates. On the other hand, the bankfull channel widths corresponding to larger cross sections tend to be somewhat underpredicted, while smaller cross-section widths (approximately <10 m) appear to be overpredicted. This latter result is likely due to the effects of slump blocks, not considered in the present modeling framework, which however play a nonnegligible role in relatively narrow channels (Parker et al., 2011). On the other hand, when the river becomes very large, the height of the banks increases in order to accommodate the larger flow depths (Figure 9b). Consequently, the stability of the banks is likely controlled by geothecnical stability, rather than by grain erosion. In addition, field observations suggest that large low-slope sand-bed rivers likely do not make the transition from dunes to a flat bed at shear stresses as low as those observed in laboratory flumes (Julien and Klaassen, 1995; Wright and Parker, 2005). Equation 7 tends thus to overpredict the Chezy coefficient and, hence, to underpredict the overall bed shear stress, eventually leading to smaller values of the equilibrium width.

5. Discussion

The universal relationships (26)–(27) have been obtained by assuming that the effective shear stress responsible for bank erosion is controlled by the presence of a sequence of bumps on the bank surface, determining the partitioning of the total shear stress τ_T into skin friction τ_{sf} and form drag τ_D contributions. The equilibrium cross-section width is assumed to be attained when the skin friction shear stress equals the critical shear stress for particle erosion. Since τ_{sf} is in general found to be about 0.3–0.4 τ_T, for a given discharge the resulting equilibrium width is definitely smaller than that obtained by neglecting the presence of bank

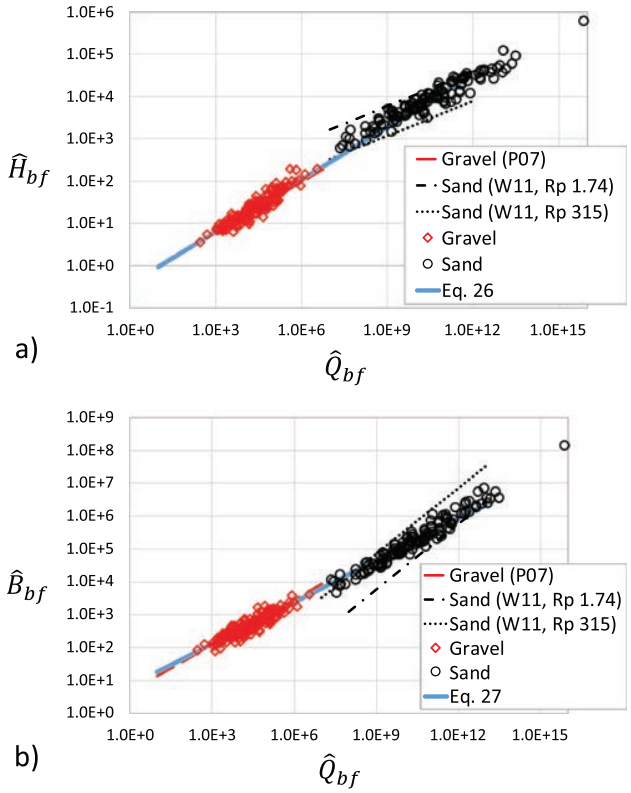

Figure 10. Comparison of the universal relations (26)–(27) with those derived empirically through linear regression and back data analysis by Parker et al. (2007) for gravel-bed rivers (P07) and by Wilkerson and Parker (2011) for sand-bed rivers (W11), for two different values of particle Reynolds number, R_p.

surface disturbances. In order to test this modeling framework, we compare equations (26)–(27) with the quasi-universal relationships derived by Parker et al. (2007) and Wilkerson and Parker (2011) from back calculation of the relevant exponents and coefficients from data for gravel and sand rivers, respectively. The comparison is carried out by rewriting equations (26)–(27) in terms of the dimensionless variables $\hat{B}_{bf}$ (= B_{bf}/D_{50}), $\hat{H}_{bf}$ (= H_{bf}/D_{50}), and $\hat{Q}_{bf}$ (see equation (22)).

The results of this comparison, shown in Figure 10, illustrate that when considering the present approach the points tend to follow a power law relationship with a constant exponent, independent of the river bed type, sand or gravel. Conversely, the semiempirical relations derived by Parker et al. (2007) and Wilkerson and Parker (2011) suggest a change of slope when considering either gravel or sand rivers. In particular, in the case of $\hat{B}_{bf}$, the exponent resulting from the present approach is 0.4429, which is very similar to the value 0.467 proposed by Parker et al. (2007) for gravel rivers, but much lower than the value 0.669 obtained by Wilkerson and Parker (2011) for sand rivers. In the case of $\hat{H}_{bf}$, the present approach suggests an exponent of 0.3450, whereas the relationships by Parker et al. (2007) and Wilkerson and Parker (2011) yield power law exponents equal to 0.3996 and 0.276 for gravel and sand rivers, respectively. Note also that the relation by Wilkerson and Parker (2011) for sand bed rivers is quite sensitive to the value of the particle Reynolds number R_p.

Figure 10 thus suggests that the bankfull geometry of both gravel and sand rivers with cohesive banks can be successfully described through a universal relationship. This indirectly confirms that the representative bump height controls, through skin friction, bank erosion and, ultimately, the equilibrium bankfull geometry of both sand-bed and gravel-bed rivers. In other words, for a given bankfull discharge, the fact that only a part of the overall shear stress (the skin friction component) contributes to fluvial erosion implies the attainment of an equilibrium width and of a flow depth quite similar to those observed in the field. This result also requires the specification of physically reasonable values of the critical shear stress for bank erosion and suitable predictors of the flow resistance exerted by the channel bed. Finally, the equilibrium sediment discharge is that dictated by the shear stress acting on the channel bed. Importantly, the present physics-based framework does not need to invoke any additional constraint as in extremal formulations, for example, minimum energy Huang et al. (2004) or maximum sediment-transport efficiency Millar (2005). Clearly, many other processes may influence the scatter of data with respect to the proposed power laws (26)–(27). In the presence of relatively high banks, the critical condition for bank collapse also depends on geotechnical stability. Various mechanisms, such as cantilever collapse, scour at the bank toe, or weathering, can promote bank failure and hence control equilibrium width. In addition, the presence of slump blocks, protecting the bank toe from the action of the river flow, is likely to affect the equilibrium width of smaller cross sections. Finally, the geometry of bump undulations is accounted for only on average, through representative values of their height and assuming a Gaussian form. Similarly, the values of the critical shear stress for erosion can strongly depend on the heterogeneity of the sediment composing the banks, as well as on vegetation cover. Hence, spatial variations of the distribution of bank undulations and of τ_c can also affect the equilibrium cross-sectional bankfull width and depth, explaining the scatter of observed data with respect to predicted values.

6. Concluding Remarks

In this paper we focused on the modeling of physical processes that lead to the widening of a river, eventually determining its equilibrium width and depth. Specifically, we considered the case whereby the width of a single-thread river channel at bankfull flow conditions is mainly controlled by fluvial erosion. The retreat of the banks is determined by the resistance of the bank material and by the presence of roughness elements

(bumps), which crucially affects the partitioning of the total shear stress into a form drag component and a skin friction component. This latter component, computed through the procedure developed by Kean and Smith (2006a), is assumed to be responsible for bank erosion and, ultimately, to control the cross-section equilibrium configuration. Even though the physical processes that can produce bank erosion may differ either in gravel or in sand bed rivers (grain erosion vs. mass or bank layer erosion), in the context of the present approach they are embedded into a critical shear stress taken to be representative of the overall bank resistance.

We thus proposed an unified modeling framework (Cross-Section Evolution Model—CSEM), valid for both sand- and gravel-bed rivers, that can be used in large variety of conditions to predict the equilibrium bankfull width and depth of a river reach on the basis of the flow discharge, the bed slope, the median sediment grain size of the channel bed, the resistance to erosion of the cohesive bank material, and the geometric properties of the undulations (bumps) present on the bank surface. The overall shear stress that the channel flow exerts on the banks, eventually driving the skin friction component responsible for fluvial erosion, is computed by coupling the central flow region with the bank flow regions. The possible presence of bed forms on the channel bed is also accounted for, by applying a suitable dune formation criterion and considering their effective roughness height. The form drag induced by the bumps implies that only a certain amount of the total shear stress (the skin friction component) contributes to bank erosion and, hence, to cross-section widening when the cross section is narrower than its equilibrium width B. As a consequence, the model predicts values of B that generally match the observed ones, without the need to invoke other processes, such as the armoring of the bank by slump blocks. Finally, the present model allows determining the equilibrium width through the progressive widening of an initially narrow section; however, it could be easily modified to account for in-channel sediment deposits, which could form near to the banks and are subsequently consolidated by vegetation encroachment, thus allowing to evaluate the attainment of an equilibrium width starting from a wider channel.

The application of the CSEM model to a large data set concerning the features of rivers at bankfull conditions led us to express the critical shear stress at the bank (equation (23)) and the average height of the bumps (equation (24)) as a function of the bankfull discharge. These relations have been subsequently used in conjunction with the CSEM model to derive the universal relationships (i.e., valid for both gravel and bed rivers) for predicting the flow depth (26) and the cross-section river width (27).

The CSEM model turns out to be quite robust. When tested against an independent set of data, it generally provides reliable estimates of bankfull channel depth and width for both sand- and gravel-bed rivers. The systematic errors that are found to affect the smaller width ($B < 10$ m, which are overestimated) and the larger widths ($B > 500$ m, which tend to be underestimated) can be explained by the presence of other mechanisms, concomitant to fluvial erosion, that can be attributed to bank collapse (in the case of higher banks) or protection of the banks exerted by sediment deposits (such as the slump blocks in the case of relatively narrow rivers).

In summary, the morphological relations (26) and (27) perform optimally in a wide range of flow discharges and sedimentological conditions. The above discussed upper and lower limiting values of B for which they tend to underperform are not rigid, and they are intended more as a caveat for an informed use of the proposed relations and of the CSEM model they are derived through.

Appendix A: Outline of Kean and Smith Approach

We briefly summarize the relevant equations of the model developed by Kean and Smith (2006a),Kean and Smith (2006b). We refer the reader to the original paper for further details.

The theoretical framework assumes that the macroroughness of the bank surface associated with the presence of a wavy bump can be approximated by equivalent undulations of Gaussian shape, with given height, streamwise length and element spacing (Kean and Smith, 2006b). Owing to the presence of these bumps, the flow field near the bank consists of an internal boundary layer region, a wake region, and an outer boundary layer region (Figure A1). FA1

The total shear stress on the bank is decomposed as the sum of the skin and form drag stresses:

$$\tau_T = \tau_{sf} + \tau_d, \tag{A1}$$

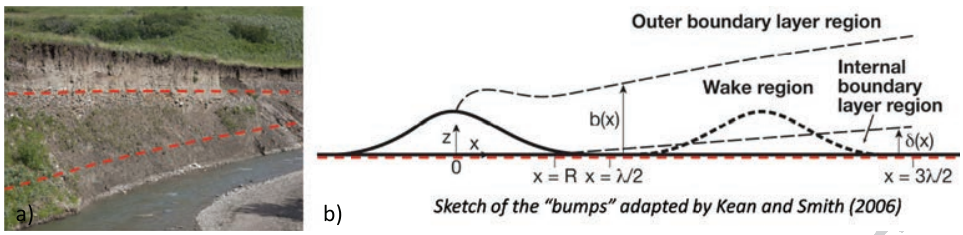

Figure A1. (a) Bump distribution along a bank of the Cecina River; (b) sketch of the equivalent Gaussian sequence used to approximate the actual spatial distribution. The sketch also depicts the structure of the wake region, as well as of internal and outer boundary layer regions.

where

$$\tau_{sf} = \rho\langle u_{*IBL}\rangle^2; \qquad \tau_d = \frac{1}{2}\rho\, C_D \frac{H}{\lambda} u_{ref}^2. \tag{A2}$$

The drag coefficient C_D is evaluated empirically though the relation:

$$C_D = 1.79 \;\; exp\left(-0.77\frac{\sigma}{H}\right), \tag{A3}$$

while the shear velocity u_{*IBL} within the internal boundary layer is estimated as $\sqrt{\tau_{IBL}/\rho} \approx \sqrt{\tau_{sf}/\rho}$. Here, τ_{IBL} is the local skin friction shear stress in the absence of bumps, which can be approximated with the shear stress due to local grain roughness (τ_{sf}). The reference velocity u_{ref}^2 is obtained by integrating the flow velocity across the plan view area A of the equivalent Gaussian shaped element:

$$u_{ref}^2 = \frac{1}{A}\int_A u^2(x,z)\; dA. \tag{A4}$$

The velocity $u^2(x,z)$ within the internal boundary layer is approximated through the law of the wall, while in the wake region the far-field wake solution of Hermann et al. (1979) is employed. We refer the reader to (Kean and Smith, 2006a) for the specific expressions attained by u in these two regions and the related coefficients. Here we simply recall that the model requires as input data: the geometrical characteristics of the equivalent Gaussian bump elements $(H_{reg}, \sigma_{reg}, \lambda_{reg})$ used to characterize, on average, the spatial distribution of macroroughness on the bank surface; the local, small-scale roughness height of bank material z_{0SF} (essentially related to the larger sediment grains, and for our simulations assumed constant and equal to $0.0005m$); the flow velocity of the outer boundary layer u_{out} at a prescribed distance from the bank z_{crit}. As an output, besides the shear stresses τ_T, τ_{sf}, and τ_d, the model also gives the roughness height z_{0T} due to skin friction and form drag that, for a regular sequence of bumps, reads

$$z_{0T} = z_m \exp\left\{-\kappa\frac{u_b}{u_{*T}}\left[1 - g(x_c)\; f\left(\frac{z_m}{b(x_c)}\right)\right]\right\}, \tag{A5}$$

with z_m matching level between wake and outer flow region, u_b velocity at the top of the wake, $g(x)$ and $f(z)$ are structure functions in wake solution, $b(x)$ is the wake thickness, and x_c is the position of the crest element.

Notation

0	subscript for central region of the flow
bf	subscript for bankfull condition
LT	subscript for lower triangle region of the flow (Figure 2)
UT	subscript for upper triangle region of the flow (Figure 2)
A	liquid area for the various cross-section regions
A_d	amplitude of dunes on the channel bed
B	channel width
C	Chezy friction coefficient in the various cross-section regions
D_{50}	median grain size of bed sediment
D_{90}	grain diameter such that 90% of the material is finer (bed sediment)
e_s	effective channel roughness

Fr	Froude number
g	gravity acceleration
H_{bf}	bankfull flow depth
H_{reg}	height of equivalent elements of regular bump sequence
k	von Karman constant
Q	flow discharge
R	hydraulic radius
U	mean longitudinal velocity in the various cross-section regions
$u(y)$; $u(z)$	longitudinal velocity profiles in directions normal to the channel bed and banks
u_*	friction velocity
S	longitudinal channel slope
y	vertical coordinate normal to the channel bed
y_{0T}	reference level where the velocity normal to the channel bed vanishes
z	transverse coordinate orthogonal to the bank
z_{0sf}	roughness height due to skin friction on channel banks
z_{out}	width of the wall boundary layer on channel banks
z_{0T}	roughness height due to skin friction plus form drag on channel banks
ϵ	rate of fluvial bank erosion
λ_{reg}	spacing of elements of regular bump sequence
λ_d	length of dune of channel bed
σ_{reg}	streamwise length scale of elements of regular bump sequence
τ_{bf}	overall bed shear stress for bankfull conditions
τ_c	critical shear stress for bank sediment erosion
τ_d	form drag stress acting on the banks
τ_{sf}	skin friction stress acting on the banks
τ_T	total shear stress exerted on the banks

Acknowledgments
Daniel Macovei and Gianni Della Monica are acknowledged for preliminary analysis of data. Steve Darby and Massimo Rinaldi are acknowledged for fruitful discussion on fluvial erosion processes and bank characterization, which deeply inspired this work. The complete data set of Tables 2 and 3 of the paper and the source files of CSEM code are archived in a public domain repository (at DOI: 10.5281/zenodo.3359005).

References

Ackers, P., & White, W. R. (1973). Sediment transport: New approach and analysis. *Journal of the Hydraulics Division of American Society Civil Engineering*, *99*, 2041–2060.
Amiri-Tokaldany, E., Darby, S. E., & Tosswell, P. (2003). Bank stability analysis for predicting reach scale land loss and sediment yield. *Journal of the American Water Resources Association*, *39*(4), 897–909.
Andrews, E. D. (1984). Bed material entrainment and hydraulic geometry of gravel-bed rivers in Colorado. *Geological Society of America Bulletin*, *95*, 371–378.
Arulanandan, K., E. Gillogley, and R. Tully (1980), Development of a quantitative method to predict critical shear stress and rate of erosion of natural undisturbed cohesive soils., Tech. Rep. GL-80-5, DTIC Document, Davis, CA (USA).
Bagnold, R.A. (1966), An approach to the sediment transport problem from general physics, US Geol. Survey Prof. Paper 422-I, Washington, D.C.
Blench, T. (1957). *Regime behaviour of canals and rivers.* Butterworths Scientific Publications London.
Blom, A., Arkesteijn, L., Chavarrias, V., Viparelli, E., & E. (2017). The equilibrium alluvial river under variable flow and its channel-forming discharge. *Journal of Geophysical Research: Earth Surface*, *122*, 1924–1948. https://doi.org/10.1002/2017JF004213
Bressan, F., Wilson, C. G., & Papanicolaou, A. N. (2014). Improved streambank countermeasures: The Des Moines River (USA) case study. *International Journal of River Basin Management*, *12*(1), 69–86. https://doi.org/10.1080/15715124.2014.882844
Buffington, J. M. (2012). Changes in channel morphology over human time scales. In M. Church, P. M. Biron, & A. G. Roy (Eds.), *Gravel-bed Rivers: Processes, Tools, Environments* (pp. 435–463). Wiley, Chichester, UK..
Buffington, J. M., & Montgomery, D. R. (1999). Effects of hydraulic roughness on surface textures of gravel-bed rivers. *Water Resources Research*, *35*(11), 3507–3521. https://doi.org/10.1029/1999WR900138
Cao, S., & Knight, D. (1998). Design for hydraulic geometry of alluvial channels. *Journal of Hydraulic Engineering*, *124*(5), 484–492.
Chang, H. H. (1979). Minimum stream power and river channel patterns. *Journal of Hydrology*, *41*(3-4), 303–327.
Chang, H. H. (1980a). Geometry of gravel streams, *ASCE*. *Journal of the Hydraulics Division*, *106*(9), 1443–1456.
Chang, H. H. (1980b). Stable alluvial canal design, *ASCE*. *Journal of the Hydraulics Division*, *106*(5), 873–891.
Colombini, M., & Tubino, M. (1991). Finite-amplitude free bars: A fully non-linear spectral solution. In R. Soulsby, & R. Bettes (Eds.), *Sand transport in rivers, estuaries and the sea* (Vol. 262, pp. 163–169). Brookfield, VT: A. A. Balkema.
Dade, W. B., & Friend, P. F. (1998). Grain-size, sediment-transport regime, and channel slope in alluvial rivers. *The Journal of Geology*, *106*, 661–675.
Darby, S., & Thorne, C. (1995). Effect of bank stability on geometry of gravel rivers. *Journal of Hydraulic Engineering*, *121*(4), 382–384. https://doi.org/10.1061/(ASCE)0733-9429(1995)121:4(382)
Darby, S., Trieu, H., Carling, P., Sarkkula, J., Koponen, J., Kummu, M., et al. (2010). A physically based model to predict hydraulic erosion of fine-grained riverbanks: The role of form roughness in limiting erosion. *Joural of Geophysical Research*, *115*, F04003. https://doi.org/10.1029/2010JF001708
Davies, T., & Sutherland, A. (1980). Resistance to flow past deformable boundaries. *Earth Surface Processes*, *5*(2), 175–179.
Diplas, P., & Vigilar, G. (1992). Hydraulic geometry of threshold channels. *Journal of Hydraulic Engineering*, *118*(4), 597–614.

Einstein, H. A.(1950), The bed-load function for sediment transportation in open channel flows, Technical Bulletin, U.S. Department of Agriculture, Soil Conservation Service, 1026.
Ferguson, R. I. (1986). Hydraulics and hydraulic geometry. *Progress in Physical Geography*, *10*(1), 1–31.
Garcia, M. H. (2000). The legend of A. F Shields, discussion. *Journal of Hydraulic Engineering*, *126*(9), 718–719.
Glover, R. E., and Q. Florey (1951), Stable channel profiles (Hydraulic Laboratory Report Hyd-325), US Bureau of Reclamation, Design and Construction Division.
Griffiths, G. A. (1984). Extremal hypotheses for river regime: An illusion of progress. *Water Resources Research*, *20*(1), 113–118.
Grissinger, E. (1982), Bank erosion of cohesive materials, Gravel-bed rivers, pp. 273–287.
Hanson, G., & Simon, A. (2001). Erodibility of cohesive streambeds in the loess area of the midwestern USA. *Hydrological Processes*, *15*(1), 23–38.
Hermann, S., et al. (1979). *Boundary layer theory*, *McGarw-Hill Book Company* (Vol. 135–149).
Hey, R. D., & Thorne, C. R. (1986). Stable channels with mobile gravel beds. *Journal of Hydraulic Engineering*, *112*(8), 671–689.
Hopson, T. M. (1999), The form drag of large natural vegetation along the banks of open channels, M.S. thesis, 114 p., Univ of Colorado, Boulder.
Huang, H. Q., Chang, H. H., & Nanson, G. C. (2004). Minimum energy as the general form of critical flow and maximum flow efficiency and for explaining variations in river channel pattern. *Water Resources Research*, *40*, W04502. https://doi.org/10.1029/2003WR002539
Ikeda, S., & Izumi, N. (1991). Stable channel cross sections of straight sand rivers. *Water Resources Research*, *27*(9), 2429–2438.
Ikeda, S., Parker, G., & Kimura, Y. (1988). Stable width and depth of straight gravel rivers with heterogeneous bed materials. *Water Resources Research*, *24*(5), 713–722. https://doi.org/10.1029/WR024i005p00713
IML-CZO (Intensively Managed Landscapes - Critical Zone Observatory), (2014), Data storage facility. http://data.imlczo.org/
Inglis, C. C. (1949), The behaviour and control of rivers and canals (with the aid of models) (Research Publication 13), Poona, India: Central Waterpower Irrigation and Navigation Research Station.
Jepsen, R., Roberts, J., & Gailani, J. (2010). Effects of bed load and suspended load on separation of sands and fines in mixed Sediment. *Journal of Waterway, Port, Coastal, and Ocean Engineering*, *136*(6), 319–326.
Julian, J. P., & Torres, R. (2006). Hydraulic erosion of cohesive riverbanks. *Geomorphology*, *76*(1), 193–206.
Julien, P. Y., & Klaassen, G. (1995). Sand dune geometry of large rivers during floods. *Journal of Hydraulic Engineering*, *121*(9), 657–663.
Kean, J., & Smith, J. (2006a). Form drag in rivers due to small-scale natural topographic features: 1 Regular sequences. *Journal of Geophysical Research*, *111*, F04009. https://doi.org/10.1029/2006JF000467
Kean, J., & Smith, J. (2006b). Form drag in rivers due to small-scale natural topographic features: 2 Irregular sequences. *Journal of Geophysical Research*, *111*, F04010. https://doi.org/10.1029/2006JF000490
Knighton, D. (1998). *Fluvial forms and processes*. London: Edward Arnold.
Kovacs, A., & Parker, G. (1994). A new vectorial bedload formulation and its application to the time evolution of straight river channels. *Journal of Fluid Mechanics*, *267*(6), 153–183. https://doi.org/10.1017/S002211209400114X
Lacey, G. (1930), Stable channels in alluvium, in Minutes of the Proceedings of the Institution of Civil Engineers (Great Britain, 229, 259–292.
Lagasse, P.F., W. J. Spitz, L. W. Zevenbergen and D. W. Zachmann (2004), Handbook for Predicting Stream Meander Migration,, *NCHRP Rep*. (533), Washington, D.C.
Lane, E. W. (1955). Design of stable channels. *Transactions of the American Society of Civil Engineers*, *120*(1), 1234–1260.
Leopold, L. B., and W. B. Langbein (1962), The concept of entropy in landscape evolution, Prof. Pap., 500A, Washington, DC: U.S. Geological Survey.
Leopold, L. B., and T. Maddock, Jr. (1953), The hydraulic geometry of stream channels and some physiographic implications, Prof. Pap., 252.
Leyland, J., Darby, S. E., Teruggi, L., Rinaldi, M., & Ostuni, D. (2015). A self-limiting bank erosion mechanism? Inferring temporal variations in bank form and skin drag from high resolution topographic data. *Earth Surface Processes and Landforms*, *40*(12), 1600–1615.
Li, C., Czapiga, M. J., Eke, E. C., Viparelli, E., & Parker, G. (2015). Variable shields number model for river bankfull geometry: Bankfull shear velocity is viscosity-dependent but grain size-independent. *Journal of Hydraulic Research*, *53*(1), 36–48.
Lindley, E. (1919), Regime channels, in Proc. Punjab Engng Cong. 7, vol. 262, p. 63–74.
Lundgren, H., & Jonsson, I. G. (1964). Shear and velocity distribution in shallow channels. *ASCE Journal of the Hydraulics Division*, *90*(1), 1–21.
Marchi, E. (1961). Il moto uniforme delle condotte liquide nei condotti chiusi e aperti. *L'Energia Elettrica*, *5*, 393–413.
McLean, S., & Smith, J. D. (1986). A model for flow over two-dimensional bed forms. *Journal of Hydraulic Engineering*, *112*(4), 300–317.
Millar, R. G. (2005). Theoretical regime equations for mobile gravel-bed rivers with stable banks. *Geomorphology*, *67*, 204–220.
Mosselman, E. (1998). Morphological modelling of rivers with erodible banks. *Hydrological Processes*, *12*(8), 1357–1370.
Nardi, L., & Rinaldi, M. (2010). Modelling riverbank retreat by combining reach-scale hydraulic models with bank-scale erosion and stability analyses. In *River Flow* (pp. 1285–1291). Braunschweig: Bundesanstalt für Wasserbau.
Nash, J. E., & Sutcliffe, J. V. (1970). River flow forecasting through conceptual models Part I—A discussion of principles. *Journal of Hydrology*, *10*(3), 282–290. https://doi.org/10.1016/0022-1694(70)90255-6
Neill, C. (1968), A re-examination of the beginning of movement for coarse granular bed materials, (Int. 68). Wallingford, England: Hydraulics Research Station.
Papanicolaou, A. N., S. Dey, M. Rinaldi, and A. Mazumdar (2006), Research issues for riverine bank stability analysis in the 21st century. Rep. 457, Obermann Center, Univ. of Iowa, Iowa City, IA.
Papanicolaou, A. N., Elhakeem, M., & Hilldale, R. (2007). Secondary current effects on cohesive river bank erosion. *Water Resources Research*, *43*(12), W12418. https://doi.org/10.1029/2006WR005763
Papanicolaou, A. N., Wilson, C. G., Tsakiris, A. G., Sutarto, T., Bertrand, F., Rinaldi, M., et al. (2017). Understanding mass fluvial erosion along a bank profile: Using PEEP technology for quantifying retreat lengths and identifying event timing. *Earth Surface Processes and Landforms*, *42*, 1717–1732. https://doi.org/10.1002/esp.4138
Parker, G. (1978a). Self-formed straight rivers with equilibrium banks and mobile bed. Part 2 The gravel river. *Journal of Fluid Mechanics*, *89*(1), 127–146. https://doi.org/10.1017/S0022112078002505
Parker, G. (1978b). Self-formed straight rivers with equilibrium banks and mobile bed. Part 1 The sand-silt river. *Journal of Fluid Mechanics*, *89*(1), 109–125. https://doi.org/10.1017/S0022112078002499
Parker, G., Shimizu, Y., Wilkerson, G. V., Eke, E. C., Abad, J. D., Lauer, J. W., et al. (2011). A new framework for modeling the migration of meandering rivers. *Earth Surface Processes and Landforms*, *36*(1), 70–86.

Parker, G., Toro-Escobar, C. M., Ramey, M., & Beck, S. (2003). Effect of floodwater extraction on mountain stream morphology. *Journal of Hydraulic Engineering*, *129*(11), 885–895.
Parker, G., Wilcock, P., Paola, C., Dietrich, W., & Pitlick, J. (2007). Physical basis for quasi-universal relations describing bankfull hydraulic geometry of single-thread gravel bed rivers. *Journal of Geophysical Research*, *112*, F04005. https://doi.org/10.1029/2006JF000549
Partheniades, E. (1965). Erosion and deposition of cohesive soils. *ASCE Journal of the Hydraulics Division*, *91*(1), 105–139.
Pfeiffer, A. M., Finnegan, N. J., & Willenbring, J. K. (2017). Sediment supply controls equilibrium channel geometry in gravel rivers. *PNAS*, *114*(13), 3346–3351.
Pickup, G. (1976). Adjustment of stream-channel shape to hydrologic regime. *Journal of Hydrology*, *30*(4), 365–373.
Pizzuto, J. (1990). Numerical simulation of gravel river widening. *Water Resources Research*, *26*(9), 1971–1980. https://doi.org/10.1029/WR026i009p01971
van Rijn, L. C. (1984). Sediment transport, Part III: Bed forms. *Journal of Hydraulic Engineering*, *110*(12), 1733–1754.
Rinaldi, M., & Darby, S. E. (2007). Modelling river-bank-erosion processes and mass failure mechanisms: Progress towards fully coupled simulations. *Developments in Earth Surface Processes*, *11*, 213–239.
Samadi, A., Amiri-Tokaldany, E., & Darby, S. (2009). Identifying the effects of parameter uncertainty on the reliability of riverbank stability modelling. *Geomorphology*, *106*(3), 219–230.
Shields, A. (1936). Anwendung der Aehnlichkeitsmechanik und der Turbulenzforschung auf die Geschiebebewegung. In *Mitteilungen der Preussischen Versuchsanstalt für Wasserbau und Schiffba, Heft(26)*. Berlin (in German).
Simons, D., & Albertson, M. (1963). Uniform water conveyance channel in alluvial material. *Trans ASCE*, *128*(1), 65–107.
Smith, J. D., & McLean, S. (1977). Spatially averaged flow over a wavy surface. *Journal of Geophysical Research*, *82*(12), 1735–1746.
Sutarto, T., Papanicolaou, A. N., Wilson, C. G., & Langendoen, E. J. (2014). Stability analysis of semi-cohesive stream banks with CONCEPTS: Coupling field and laboratory investigations to quantify the onset of fluvial erosion and mass failure. *Journal of Hydraulic Engineering*, *140*(9), 04014041. https://doi.org/10.1061/(ASCE)HY.1943‐7900.0000899
Thorne, S. D., & Furbish, D. J. (1995). Influences of coarse bank roughness on flow within a sharply curved river bend. *Geomorphology*, *12*(3), 241–257.
Tolhurst, T., Black, K., Shayler, S., Mather, S., Black, I., Baker, K., & Paterson, D. (1999). Measuring the in situ erosion shear stress of intertidal sediments with the cohesive strength meter (CSM). *Estuarine, Coastal and Shelf Science*, *49*(2), 281–294.
Trampush, S., Huzurbazar, S., & McElroy, B. (2014). Empirical assessment of theory for bankfull characteristics of alluvial channels. *Water Resources Research*, *50*, 9211–9220. https://doi.org/10.1002/2014WR015597
White, W. R., Bettess, R., & Paris, E. (1982). Analytical approach to river regime. *ASCEJournal of the Hydraulics Division*, *108*(10), 1179–1193.
Wilkerson, G., & Parker, G. (2011). Physical basis for quasi-universal relationships describing bankfull hydraulic geometry of sand-bed rivers. *Journal of Hydraulic Engineering*, *137*(7), 739–753. https://doi.org/10.1061/(ASCE)HY.1943-7900.0000352
Wilson, C. G., Papanicolaou, A. N., & Abaci, O. (2009). SOM dynamics and erosion in an agricultural test field of the Clear Creek IA watershed. *Hydrology and Earth System Sciences Discussions*, *6*, 1–39.
Wright, S., & Parker, G. (2005). Flow resistance and suspended load in sand-bed rivers: Simplified stratification model. *Journal of Hydraulic Engineering*, *130*(8), 796–805. https://doi.org/10.1061/(ASCE)0733-9429(2004)130:8(796)
Yalin, M. (1971). *Theory of hydraulic models*. London: Macmillan.
Yalin, M., & Ferreira Da Silva, A. (2000). Computation of regime channel characteristics on thermodynamic basis. *Journal of Hydraulic Research*, *38*(1), 57–63.
Yang, C. T. (1971). On river meanders. *Journal of Hydrology*, *13*, 231–253.
Yang, C. T., & Song, C. (1979). Theory of minimum rate of energy dissipation. *ASCE Journal of the Hydraulics Division*, *105*(7), 769–784.
Yang, C. T., Song, C., & Woldenberg, M. J. (1981). Hydraulic geometry and minimum rate of energy dissipation. *Water Resources Research*, *17*(4), 1014–1018.
Yen, B. C. (2002). Open channel flow resistance. *Journal of Hydraulic Engineering*, *218*(1), 20–29.